The Journal of Chemical Physics

Non-monotonic response of a sheared magnetic liquid crystal to a continuously increasing external field

Cite as: J. Chem. Phys. **152**, 024505 (2020); https://doi.org/10.1063/1.5126398
Submitted: 02 September 2019 . Accepted: 23 December 2019 . Published Online: 14 January 2020

Nima H. Siboni, Gaurav P. Shrivastav, and Sabine H. L. Klapp

The Journal of Chemical Physics ARTICLE scitation.org/journal/jcp

Non-monotonic response of a sheared magnetic liquid crystal to a continuously increasing external field

Cite as: J. Chem. Phys. 152, 024505 (2020); doi: 10.1063/1.5126398
Submitted: 2 September 2019 • Accepted: 23 December 2019 •
Published Online: 14 January 2020

Nima H. Siboni,[1,a)] Gaurav P. Shrivastav,[2] and Sabine H. L. Klapp[1]

AFFILIATIONS

[1] Institut für Theoretische Physik, Technische Universität Berlin, Hardenbergstraße 36, 10623 Berlin, Germany
[2] Institute für Theoretical Physics, Technische Universität Wien, Wiedner Hauptstr. 8-10, 1040 Vienna, Austria

[a)] **Electronic mail:** hamidisiboni@tu-berlin.de

ABSTRACT

Utilizing molecular dynamics simulations, we report a nonmonotonic dependence of the shear stress on the strength of a continuously increasing (i.e., time-varying) external magnetic field (H) in a liquid-crystalline mixture of magnetic and nonmagnetic anisotropic particles. We relate the origin of this nonmonotonicity of the transient dynamics to the competing effects of particle alignment along the shear-induced direction, on the one hand, and the magnetic field direction, on the other hand. To isolate the role of these competing effects, we consider a two-component mixture composed of particles with effectively identical steric interactions, where the orientations of a small fraction, i.e., the magnetic ones, are coupled to the external magnetic field. By increasing H from zero, the orientations of the magnetic particles show a Fréederickz-like transition and eventually start deviating from the shear-induced orientation, leading to an increase in shear stress. Upon further increase of H, a demixing of the magnetic particles from the nonmagnetic ones occurs, which leads to a drop in shear stress, hence creating a nonmonotonic response to H. Unlike the equilibrium demixing phenomena reported in previous studies, the demixing observed here is neither due to size-polydispersity nor due to a wall-induced nematic transition. Based on a simplified Onsager analysis, we rather argue that it occurs solely due to packing entropy of particles with different shear- or magnetic-field-induced orientations.

I. INTRODUCTION

As proposed in a seminal work[1] by Brochard and de Gennes, doping liquid crystals (LC) with magnetic nanoparticles (MNP) leads to remarkable hybrid materials whose properties can be controlled by an external magnetic field. These stimuli-responsive materials exhibit rich self-assembly in equilibrium and show marked effects under external fields.[2–7] A key factor in determining these emergent properties is the shape of the MNP:[7–9] Commonly, the MNP are either spherical (and hence different from the LC), or they are anisotropic with a large size disparity between the MNP and LC particles.[6,7,10,11] In this paper, we investigate, on a computational basis, mixtures where the MNP are identical to LC in their anisotropy and size. This is a timely issue due to recent advances in experimental realizations of such anisotropic magnetic particles,[3,12–14] which has motivated also a number of analytical and numerical studies.[15–18]

The aforementioned studies[15–18] focus on the effect of the magnetic field on the structural and optical properties. Here, we focus on a different aspect of the response to the external field, that is, the mechanical response of the mixture. A key difference between optical and mechanical responses is that, unlike in the optical case where light is transmitted through the sample without changing the structure, a mechanical perturbation itself can lead to structural changes. In particular, when the system is sheared, this leads to shear-induced changes of the structure.[19–23] We show that these shear-induced effects combined with the magnetic field induced effects lead to an intriguing mechanical response and structural changes.

The focus of the present study is to isolate the role of the magnetic field-induced orientation of the MNP on the structure and rheology of such mixtures. To achieve this goal, we consider a mixture where not only the shape and size of the MNP and LC are identical, but also they interact via the same interparticular potential. Only the directions of the MNP are coupled to the external magnetic field, and this coupling distinguishes the MNP from the LC. The assumed monodispersity in size and uniformity in interparticular interaction has several consequences: (i) there is no specific anchoring between the LC and MNP beyond anchoring among LC and MNP; (ii) polydispersity-induced phenomena, which are by themselves subject of intensive research,[24–29] are absent here; and (iii) unlike Refs. 30–35, there is no structure formation due to the direct magnetic dipole–dipole interaction between the MNP. These properties of our model enable us to isolate the role of the selectively controlled direction of particles and study its effect on the structure and rheology of the whole system.

In pure ferrofluids, the interplay of an external magnetic field and shear leads to the well-known magnetoviscous effects (see Ref. 36 and references therein): By applying the magnetic field, the viscosity of the system strongly and monotonically increases. This monotonic increase appears even for very dilute systems, where the dipole–dipole interactions are negligible.[37–39] However, for mixtures containing anisotropic MNP, such effects are not studied, to the best of our knowledge. As a first step towards an understanding of the magnetorheological properties of this mixture, we study the response of the mixture to a monotonically increasing magnetic field. Due to the variation with time we do not have direct access to the steady-state behavior of the system. The advantage of our protocol, however, is that it enables us to scan a large range of field strengths (at different system parameters like temperature) and simultaneously avoid large computational costs. Our results show that the shear stress, and thus, the viscosity, displays an intriguing nonmonotonic dependence on the strength of the magnetic field. We analyze this shear-stress behavior by investigating its correlation to the structure of the mixture at different magnetic field values.

From methodological point of view, we use extensive nonequilibrium molecular dynamics (NEMD) simulations. Although NEMD simulations, in practice, have restrictions regarding accessible time and length scales, they nevertheless enable us to study the mixture in the presence of both shear and external magnetic field, where an analytical approach is missing. Furthermore, in NEMD simulations, no assumption on the spatial distribution of the particles is imposed, contrary to studies,[15,16] which are based on continuum theories. In these continuum models, a homogeneous distribution of MNP is assumed. Our results show that such an assumption is, in fact, not fulfilled. Indeed, we find clear evidence for the formation of an inhomogeneous spatial distribution with pronounced consequences for the mechanical response of the system.

In resemblance to the geometry of a rheometer, we shear the mixture by relative motion of two walls, and obtain the shear stress directly measuring the exerted forces on the walls. To analyze the structure of the sample, we use well-established quantities characterizing the orientational order, and also introduce a new quantity to characterize the positional distribution of MNP across the system. Using these quantities, we argue that the nonmonotonic behavior of the stress emerges as a delicate interplay between (i) an increase in stress due to orientational deviations of the MNP from the shear-induced orientation, and (ii) a decrease in stress due to an entropic demixing, which is caused by differences of the orientations of the LC and MNP.

II. SIMULATION SETUP

The simulation setup consists of ellipsoidal uniaxial Gay-Berne (GB) particles,[40] where a fraction of them have a permanent magnetic point dipole embedded in the particle center and pointing along the long axis. The system is subjected to (i) shear flow, which is realized via a relative motion of two walls between which the particles are confined, and (ii) an external magnetic field. In this section, after briefly introducing the GB parameters, the protocols for creating independent samples, shearing, and applying the external field are explained. Furthermore, the observables and the relevant dimensionless parameters are introduced. A snapshot of the system, in the isotropic state, and in the absence of the shear flow and magnetic field, is shown in Fig. 1.

For the GB potential, we adopt the notation and parameter values used in Ref. 35. Similar to Ref. 35, the simulation units are set such that the characteristic length and energy of the GB interaction, as well as particle mass are $\sigma_0 = 1$, $\varepsilon_0 = 1$, and $m = 1$, respectively. In these units, the lengths associated with semiaxes of the ellipsoids are $\sigma_s = 1$ and $\sigma_l = 3$, for the short and the long axes of the ellipsoid, respectively. In addition to the GB interaction, the magnetic ellipsoids also interact via magnetic dipole–dipole potential. In the present work, however, we are primarily interested in the effect of the interaction of the magnetic dipoles with the external field. Therefore, the dipole–dipole interaction is set to a negligible

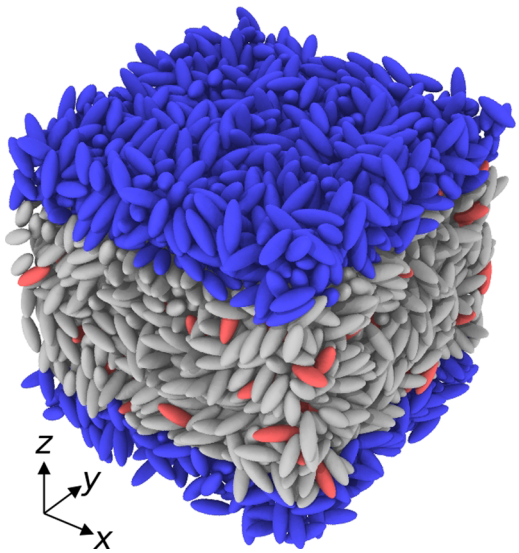

FIG. 1. A snapshot of the simulation setup in the absence of the shear and the external magnetic field: red, gray, and blue ellipsoidal particles represent magnetic, nonmagnetic, and wall particles, respectively. The sample is in an isotropic state ($T = 5$), the state from which the walls are created.

value compared to the thermal energy. Thus, under the present conditions, thermal fluctuations are dominant in the sense that they prevent formation of structures due to the magnetic dipole–dipole interaction.

The protocol to create systems similar to Fig. 1 consists of two steps: (i) independent three-dimensional configurations are created by sampling from a molecular dynamics simulation with periodic boundary conditions at high temperature, (ii) walls are created via sudden freezing of two slabs of particles. These two steps are now explained in detail.

As a first step, independent samples are created. For this purpose, an equilibrium molecular dynamics (EMD) simulation is performed with a constant number of particles, $N = 4000$, at a constant volume (a cubic box with the spatial extension $L \simeq 23$), and at a constant temperature, T. This simulation is performed with the Large-scale Atomic/Molecular Massively Parallel Simulator (LAMMPS)[41] package, where a new `fix` is introduced for embedding the point dipole moments along the longest axes of the magnetic particles. This `fix` can be found in the supplementary material for further use. We set the number of magnetic particles to $N_{\mathrm{MNP}} = 200$. Newton's equations of motion for both rotational and positional degrees of freedom are integrated using the velocity-Verlet algorithm[42,43] with the time-step $\delta t = 5 \times 10^{-3}$. The temperature is kept constant using a Langevin thermostat with the same parameters as in Ref. 35.

For the present choice of GB parameters and the number density, the equilibrium system exhibits isotropic, nematic, and smectic phases.[44,45] For the purpose of creating independent samples, we consider the case that the equilibrium system (in the absence of shear and the magnetic field) is deep in the isotropic state. We thus set the temperature to $T = 5$, which is significantly larger than the isotropic–nematic transition temperature, $T_{\mathrm{IN}} \simeq 1.5$.[44,45] To assure the independence of the configurations, the time interval between each two consecutive samplings is chosen to be large enough such that, on average, particles move almost 10 length units in that time interval.

In the second step, we create walls for each sample for the later implementation of shear flow (see Refs. 46–48 for a similar strategy). To this end, the sampling at high temperature is followed by a sudden quench of the upper and lower slabs of particles (relative to the z-direction), as depicted in Fig. 1 by blue-colored ellipsoids. As the walls are formed at high temperature, the distributions of the LC and MNP are uniform throughout the system. Therefore, the effective concentration of MNP in the walls and the remaining liquid slab is equal to the overall concentration of MNP. The MNP frozen in the walls are replaced with the LC, such that the walls are solely composed of nonmagnetic particles. The thickness of the walls is chosen to be larger than the GB potential cutoff in our simulation setup. These frozen slabs serve as solid, impenetrable, and rough walls. Furthermore, as shown in Appendix A in Fig. 9, the roughness is large enough that the velocity profile obtained under shear does not show slip.

After creating walls, the system is quenched to the desired temperature and sheared by a relative motion of the walls along the x-direction with a constant velocity, yielding a time-independent global shear rate, $\dot{\Gamma} = \Delta V_w/L$, where ΔV_w is the difference in the velocities of the two walls. One should note that the Langevin thermostat is decoupled from particle's x-coordinate to avoid the flow induced effects caused by shearing along this direction.[49] This is a common practice to employ thermostating algorithms for sheared systems.[50–56]

We now turn to the main physical quantities of interest in our study. Most important for the mechanical response is the shear stress. We calculate this quantity directly via summation of the x-component of the forces exerted by the liquid particles on the upper or lower wall particles, respectively,

$$\sigma_{xz} = \frac{1}{L^2} \sum_{i \in \mathrm{wall}} \sum_{j \in \mathrm{fluid}} \mathbf{f}_{ij,x}. \tag{1}$$

In Eq. (1), $\mathbf{f}_{ij,x}$ is the x-component of the force on particle i due to particle j, the summation over i is restricted to particles composing the upper or lower wall, and the j index runs over all fluid particles. We note that by using this method of σ_{xz} calculation, we are not relying on the assumptions behind the virial expression for pressure tensor calculation such as homogeneity (as discussed in Refs. 57 and 58), or being in equilibrium.[59] Knowing the shear stress, we can calculate the apparent viscosity[60] via $\eta_a := \sigma_{xz}/\dot{\Gamma}$. In this study, as we keep the shear rate constant, the qualitative behaviors of the shear stress and the apparent viscosity are identical. The ensemble averages of the stress and other quantities presented here are obtained by averaging over 15 to 50 independent samples.

To characterize the orientational structure of the system, we measure the tensorial order parameter,

$$\mathbf{Q}_\alpha = \frac{1}{N_\alpha} \sum_{i=1}^{N_\alpha} \frac{1}{2} \left(3 \hat{\mathbf{u}}_{\alpha,i} \otimes \hat{\mathbf{u}}_{\alpha,i} - \mathbb{I}\right), \tag{2}$$

where $\alpha \in \{\mathrm{LC}, \mathrm{MNP}\}$ denotes the type of the particles, N_α is the corresponding number of particles, $\hat{\mathbf{u}}_{\alpha,i}$ is the unit vector along the longest axis of the ith particle of type α, and $\mathbb{I}$ denotes the second-rank unit tensor. The nematic order parameter, S_α, and the direction associated with the nematic order director, $\hat{\mathbf{n}}_\alpha$, are obtained as the largest eigenvalue and the corresponding eigenvector of $\mathbf{Q}_\alpha$. The nematic director $\hat{\mathbf{n}}_\alpha$ only determines the orientation of the particles alignment (i.e., $\hat{\mathbf{n}}_\alpha$ is equivalent to $-\hat{\mathbf{n}}_\alpha$). Nevertheless, in this study, we always choose $\hat{\mathbf{n}}_\alpha$, which has a positive x-component. The nematic order parameter is equal to 0 at a completely random and isotropic state, and 1 for a perfect alignment of all particles. Based on the Maier-Saupe mean-field theory,[61–63] we consider $S_c \simeq 0.43$ as an approximate criterion for identifying the isotropic-to-nematic phase transition.

We also measure the (particle) averaged polar order parameter, P, whose instantaneous value is given by

$$P = \frac{1}{N_{\mathrm{MNP}}} \left| \sum_{i}^{N_{\mathrm{MNP}}} \hat{\mathbf{u}}_{\mathrm{MNP},i} \cdot \hat{\mathbf{n}}_{\mathrm{MNP}} \right|, \tag{3}$$

where the summation is limited only to the MNP, and μ is the dipole moment of each MNP.

In order to obtain quantitative information on the instantaneous spatial distribution of MNP and LC, we measure the number density profile $\rho_\alpha(z_0) := n_\alpha(z_0 - \delta z/2,\ z_0 + \delta z/2)/(L^2 \delta z)$ of particle type α, where n_α is the instantaneous number of those particles between planes $z = z_0 - \delta z/2$ and $z = z_0 + \delta z/2$, and $\delta z = 0.25$ is the discretization resolution along the z-axis.

The studied system is characterized by the following dimensionless parameters, whose (range of) values are mentioned in the brackets: the particle anisotropy, $\kappa = \sigma_l/\sigma_s$ {=3}, the total reduced density of $\rho^\star = N\sigma_s^3/L^3$ {= 0.34}, the GB energy scaled by the thermal energy, $\beta\varepsilon_0$ {=0.67} where $\beta = 1/(k_B T)$, the wall-to-wall distance scaled by the particle size, $\tilde{L} = L_c/\sigma_s$ {= 14}, where L_c is the channel width, the fraction of magnetic ellipsoids, $x = N_{\mathrm{MNP}}/N$ {=0.05}, the energy of dipolar coupling scaled by the thermal energy, $\lambda = \beta\mu^2/\sigma_s^3$ {= 10^{-4}}, the dipole-external field energy scaled by the thermal energy, $\tilde{H} = \beta\mu H$ {$\in [0, 35]$}, and the shear-induced time scaled by a structural relaxation time, $\dot{\Gamma}\tau_\sigma$ {= 0.05}, where $\dot{\Gamma} = 5 \times 10^{-2}$ is the imposed shear rate, and $\tau_\sigma \simeq 1$ is the time associated with decay of the stress autocorrelation in equilibrium (see Fig. 12 in Appendix C).

The above-mentioned choices of κ, $\rho^\star$, and $\beta\varepsilon_0$ are such that the corresponding pure GB system exhibits isotropic, nematic, and smectic phases over a feasible temperature range.[44,45] The value of $\tilde{L}$ is chosen to be large enough that the wall-induced effects are negligible, based on the following two tests, which are presented in more detail in Appendix A. First, we checked that for the confined system at equilibrium, S is close to the nematic order parameter of the same system without walls, as shown in Fig. 8 of Appendix A. Second, we checked that in the presence of shear, based on density and shear rate profiles, the wall effects are not dominating the system, as depicted in Fig. 9.

Finally, the magnetic field is introduced as follows: We first let the system reach its steady state under shear in the absence of the magnetic field. We denote this point as the beginning of measurement time, i.e., $t = 0$. From thereon, the magnetic field is switched on and slowly increased up to a saturation value, $H_{\max}$, with a constant rate over the simulation time $t_{\max}$, i.e., $\mathbf{H}(t) = H_{\max}\,(t/t_{\max})\hat{\mathbf{H}}$, where $\hat{\mathbf{H}}$ denotes the time-independent direction of the uniformly applied field. The value of $H_{\max}$ is chosen such that it allows for complete alignment of the magnetic particles with $\hat{\mathbf{H}}$ (here, $\mu H_{\max} = 50$). For all the simulations in this work, except those discussed in Appendix B where the effect of the rate of change, dH/dt, is examined, $t_{\max}$ is set to 7500 in reduced units. This corresponds to $\mu dH/dt = 6.6 \times 10^{-3}$ (in simulation units of energy per time) and $\beta\mu dH/dt = 4.4 \times 10^{-3}$ (in simulation units of inverse time) for $T = 1.5$.

III. RESULTS AND DISCUSSION

In discussing our results, we first report our main result, that is, the nonmonotonic behavior of the stress as a function of the applied external field, where the magnetic field increases with a constant rate. Subsequently, we correlate this mechanical behavior with the structure formation of the particles in the system. The main temperature that we consider is $T = 1.5$. We deliberately chose this temperature, which is very close to the isotropic–nematic transition, to ensure high sensitivity to the applied shear and magnetic field.

To start with, we present in Fig. 2, the response of the stress to the field strength for three different directions of $\hat{\mathbf{H}}$: (i) along $\mathbf{n}^{(0)}$, (ii) perpendicular to $\mathbf{n}^{(0)}$ in the yz-plane (vorticity direction), and (iii) perpendicular to $\mathbf{n}^{(0)}$ in the xz-plane (shear plane) with a positive z-component. Here, $\mathbf{n}^{(0)}$ indicates the nematic director of the entire system in the absence of the magnetic field (which is close to the direction of the shear flow, as discussed later). We note

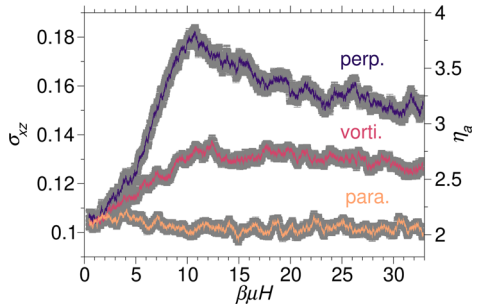

FIG. 2. Shear stress as a function of the strength of a magnetic field with three different directions: (i) the direction parallel to $\mathbf{n}^{(0)}$, (ii) the vorticity direction, which is parallel to the y-axis, and (iii) the direction perpendicular to $\mathbf{n}^{(0)}$ in the xz-plane. The left vertical axis of the graph shows the shear stress, while the right vertical axis indicates the apparent viscosity, $\eta_a = \sigma_{xz}/\dot{\Gamma}$ with $\dot{\Gamma} = 5 \times 10^{-2}$. Note that, due to our protocol, a variation of H (and consequently $\beta\mu H$) corresponds to a change in time according to $\Delta t = \Delta H(\frac{dH}{dt})^{-1}$. For all the cases, the temperature is set to $T = 1.5$, and the rate of the magnetic field increase is set such that $\beta\mu dH/dt = 4.4 \times 10^{-3}$.

that the orientation of the magnetic field is fixed and remains constant during simulation. However, as the magnetic field is increased, the nematic director of the system ($\hat{\mathbf{n}}$) changes as a result of a competition between the shear-induced and magnetic field-induced effects [thus, $\mathbf{n}^{(0)}$ deviates from the magnetic field orientation $\hat{\mathbf{H}}$, which remains along $\mathbf{n}^{(0)}$]. In our simulations, we do not fix the nematic orientation of the particles, and therefore, the obtained stress (and hence the viscosity) corresponds to the so-called apparent stress[60] (to be distinguished from common anisotropic stresses obtained by fixing the nematic director[64]). As shown in Fig. 2, the most pronounced effect of the magnetic field occurs in case (iii), where we observe, remarkably, a nonmonotonic behavior. In contrast, there are no marked field-induced changes of σ_{xz} in the parallel case. We speculate that this is because a magnetic field parallel to $\mathbf{n}^{(0)}$ does not reorient the MNP. In the present study, we restrict ourselves to case (iii) and investigate the origins of the observed nonmonotonicity as a function of the magnetic field strength $H := |\mathbf{H}|$.

The aforementioned nonmonotonic behavior is persistent, as depicted in the upper panel of Fig. 3, at the lower temperatures $T = 1.0$ and $T = 0.75$, where the corresponding equilibrium system at $H = 0$ is deep in the nematic state.[44,45] Moreover, on a qualitative level, we find the same nonmonotonic behavior also for slower and faster rates of changing H, as shown in Fig. 10 of Appendix B. Nevertheless, quantitatively, the extent of the observed nonmonotonicity is dependent on dH/dt. This suggests an interesting interplay of timescales. In the present section, we show that the two relevant processes for the nonmonotonic behavior are the orientational and positional rearrangements of the MNP. The time scales associated with these processes are estimated in Appendix B, where we also discuss their relevance for the observed behavior.

To shed light on the origin of the nonmonotonic behavior for the specific rate considered in Fig. 2, we now investigate the structure formation of the magnetic and nonmagnetic particles at different values of the magnetic field and $T = 1.5$. The corresponding

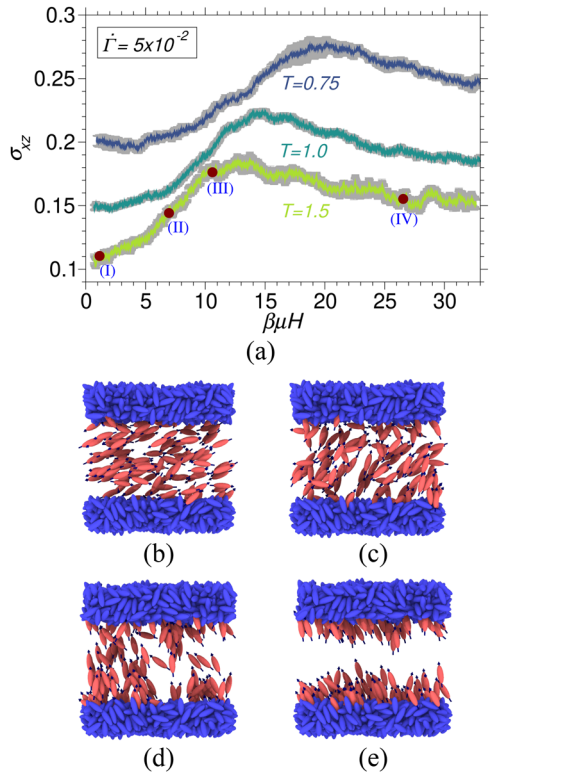

FIG. 3. Upper panel: Shear stress as a function of the magnetic field strength at three different temperatures. For visualization purposes, each curve is shifted upward vertically by 0.02 with respect to the curve with the next higher temperature. Lower panel: Representative configurations associated with the four values of the field, which are indicated by bullets and the Roman numbers on the $T = 1.5$ curve in the upper panel. For all simulations, $\dot{\Gamma}$ is kept fixed at 5×10^{-2}.

snapshots are shown in the lower panel of Fig. 3. They reveal a significant dependence of the orientational and translational structure on the external field. To quantify these magnetic field induced effects, we study, first, the structure of the system at $H = 0$, which represents our reference system. Then we show that by increasing the magnetic field to zero, the deviation of the orientations of the MNP from the shear-induced direction leads to an increase of the shear stress. By further increase of H, the aforementioned deviation increases and eventually causes demixing of the MNP and LC. Finally, we show that this demixing is correlated with the decrease of the stress at large H values.

Upon shearing the system in the absence of the magnetic field, we observe an increase in the order parameter $S_{\mathrm{LC(MNP)}}$ of particles, a phenomenon known as shear-induced ordering (see Ref. 65 and references therein). In Fig. 4, the evolution of the nematic order parameter of the system as a function of the applied strain, Γ (or, equivalently, the time interval the system is sheared), is depicted for the temperature $T = 1.5$ and shear rate $\dot{\Gamma} = 5 \times 10^{-2}$. The results show that the system evolves from a state close to isotropic–nematic transition ($S \simeq 0.45$) to a nematic state ($S = 0.65$). We recall that at $H = 0$, the LC and the MNP are essentially indistinguishable, and therefore, we report only one S for the whole system.

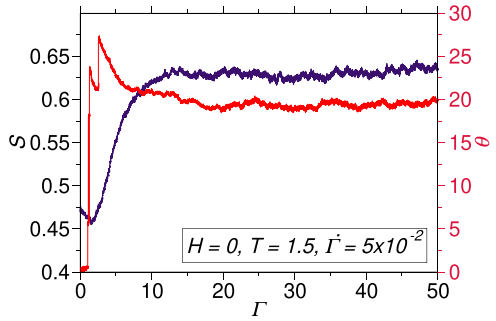

FIG. 4. Plots of the nematic order parameter, S, and the angle between the nematic order director and x-axis, θ, as functions of the strain, Γ (in the absence of the magnetic field). Shear leads to an increase in the nematic order parameter and it also changes the orientation of the director. In the absence of shear, i.e., at $\Gamma = 0$, the director is aligned parallel to the walls and upon shearing, it starts deviating from that. In the steady state, we find $\theta \simeq 20°$, which is close to the value reported in an earlier study.[66]

Applying shear not only increases the nematic order parameter, but also changes the orientation of the nematic director. In Fig. 4, the angle between the nematic director and the shear direction (i.e., x-direction) is shown: the angle θ evolves from zero to its steady state value as the strain is increased. This steady state θ value, which is also known as the Leslie angle, is $\theta \simeq 20^{\circ}$ in our system for the previously specified parameters. The obtained value, although system specific, is close to the reported value by a previous GB study.[66]

Upon increasing the magnetic field strength from zero at the finite shear ($\dot{\Gamma} = 5 \times 10^{-2}$), the MNP tend to align with $\hat{\mathbf{H}}$, inducing a competition with the shear-induced ordering along $\mathbf{n}^{(0)}$. As an illustration, we plot in Fig. 5, the nematic order parameters of each component, as well as the angles between the director of each component, $\hat{\mathbf{n}}_{\alpha}$, and the shear direction (x-direction). The nematic order parameter of the MNP, S_{MNP}, decreases for small values of H. This is since the MNP now tend to align with $\hat{\mathbf{H}}$, which is perpendicular to the nematic director in the absence of the field, i.e., $\mathbf{n}^{(0)}$, see Fig. 5(a). Interestingly, in the same range of H-values, the orientation of the nematic director is still same as for $H = 0$, as seen from the behavior of θ_{MNP} in Fig. 5(b). Indeed, the behavior of the angle between the MNP director and the shear direction is reminiscent of a Fréederickz transition:[67,68] Up to a threshold value of the external field, in this case $H_{\mathrm{th}} \simeq 5$, the director of magnetic particles is not deviating from $\mathbf{n}^{(0)}$. Upon further increase of the magnetic field, it suddenly starts deviating from $\mathbf{n}^{(0)}$, until it is fully aligned with the field direction, $\hat{\mathbf{H}}$. In this regime, increasing the magnetic field leads to an increase of S_{MNP} along the new director, as can be seen from Fig. 5(a). We note that, unlike the conventional Fréederickz transition, which is an equilibrium phenomenon, here, the system is out of equilibrium. Also, in a conventional Fréederickz transition, the unperturbed direction is induced by the confinement, whereas here, the unperturbed direction is the shear-induced direction.

The field-dependence of the ordering of magnetic particles is also reflected by the dipolar order parameter, P [see Eq. (3)], which increases from zero by applying the magnetic field. As shown in

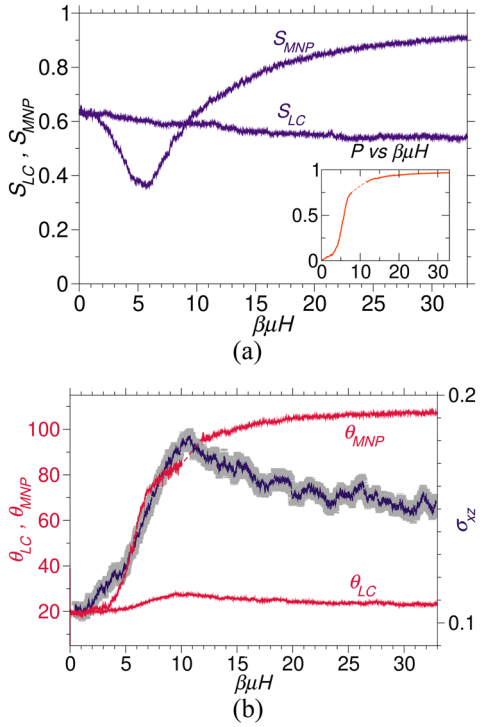

FIG. 5. (a) Nematic order parameter for LC and MNP as a function of μH. The results show that, unlike S_{MNP}, S_{LC} is not affected dramatically by the external field. The inset shows that P has a weak dependence on μH before $\mu H \simeq 5$, in contrast to its strong dependence for larger μH values. (b) The left vertical axis of the graph shows the angles between the nematic directors, i.e., $\hat{\mathbf{n}}_{LC}$ and $\hat{\mathbf{n}}_{MNP}$, with the shear direction (x-direction). The value of the these angles coincide at $H = 0$ where the LC and MNP are essentially indistinguishable. The right vertical axis of the graph shows the stress as a function of the external magnetic field strength. Similar to Fréderickz transition, up to a threshold value of the magnetic field (here, $\mu H_{th} \simeq 5$) the nematic director remains undistorted, and beyond that it starts deviating from the $H = 0$ direction, and eventually fully aligns with the direction of the magnetic field.

Fig. 5(a), a significant increase of P occurs as the magnetic field exceeds μH_{th}, although a slight increase is observed before this threshold. Here, we present a qualitative explanation of this slight increase. First, consider the case that the magnetic field is zero. Due to the elongated shape of particles, the applied shear effectively enhances the clockwise rotation of the particles (a situation similar to Ref. 69). This so-called Jeffery motion is hydrodynamic in its nature and it occurs for all MNP irrespective of the direction of their magnetic moments relative to $\mathbf{n}^{(0)}$. We note that these rotations, in zero field, cannot lead to a finite value for P. This is not anymore the case if the magnetic field is turned on: if $\hat{\mathbf{u}}$ is antiparallel to $\mathbf{n}^{(0)}$, the torque exerted by the field on the MNP tends to rotate the particle clockwise (and thus, enhancing the aforementioned shear-induced rotations). On the contrary, the shear-induced rotations are disfavored by the field for the MNP, which point parallel to $\mathbf{n}^{(0)}$. This leads to an increase of the population of the MNP, which are parallel to $\mathbf{n}^{(0)}$, and consequently, to an increase of P. This is, indeed, quite remarkable in view of the fact that the field is perpendicular to $\mathbf{n}^{(0)}$.

As is visible from Fig. 5, not only the orientational order of the MNP, but also that of the LC is affected by the magnetic field, although the LC themselves are not susceptible to the magnetic field. This is an indirect effect: The magnetic field reorients the MNP, which in turn, affects the orientation of the neighboring LC due to the anisotropic steric interactions between the MNP and LC. However, considering that the MNP form only a small fraction, the effect of the field on the LC is small at the present condition, see Fig. 5. This indirect effect gets weaker at stronger fields, which can be understood by considering the demixing between the MNP and LC, which occur for these magnetic field values. This demixing, which can be seen in snapshots presented in Fig. 6, is discussed later.

In view of the competing effects of magnetic field and shear, we are now in a position to interpret the marked nonmonotonic behavior of the shear stress, σ_{xz}. Indeed, as seen from Fig. 5(b), there is a clear correlation between the increase of σ_{xz} and the misalignment of the MNP at small to moderate values of H. This can be qualitatively understood by considering that σ is proportional to τ, where τ is the relaxation time of the system. We argue that τ increases by applying H, as applying magnetic field reduces orientational freedom of the MNP, and hence making the relaxation process less likely. Here, by the relaxation process, we refer to the atomistic mechanism behind the stress relaxation, i.e., going from a configuration with high stress to another configuration with a lower stress.[70–78] It has been argued[79–81] that the probability of such transition is proportional to the configurational entropy of the system;[79–81] roughly speaking, it is more likely for a system to make a transition, if more states are available. In the studied system here, by confining the orientation of a fraction of particles in a particular direction via magnetic field, the configurational entropy is reduced, which leads to an increase in τ and σ.

So far, we have focused on the correlation between the field-induced orientational ordering of the magnetic particles and the shear stress. Upon further increase of the magnetic field to the point, where the misalignment between MNP and LC is close to its maximum, the shear stress shows a decrease. Interestingly, this decrease occurs simultaneously with a significant qualitative change in the

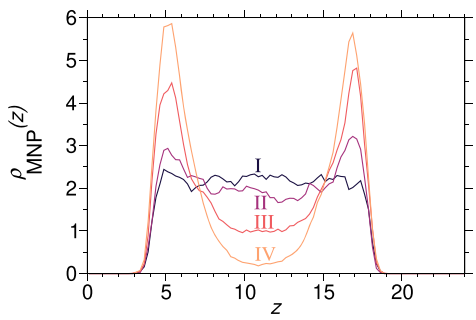

FIG. 6. The density profiles of the MNP at different magnetic field values. The roman numbers refer to the same numbers in Fig. 3. For small fields, a relatively uniform spatial distribution is obtained, in contrast to strong fields where a double-peaked profile emerges.

spatial distribution of the MNP. This qualitative change is illustrated by the four representative configurations at different values of μH, see Fig. 3: Starting from a relatively homogeneous distribution of MNP at small H, further increase of H leads to a demixing between MNP and LC. We quantify these structural transformations by measuring the averaged number density profile of MNP as a function of the external field. The results are plotted in Fig. 6: At large field strengths (state points III and IV) one observes a pronounced double-peak structure of the MNP density profile, reflecting the assembly of the MNP at the walls. This is in a qualitative contrast with the uniform spatial distribution of the MNP (and thus, also the LC) at small μH values.

To better relate the field-induced changes of the spatial distribution and the stress behavior, we introduce an entropylike measure, which quantifies the degree of inhomogeneity of the density distribution of MNP. Specifically, we consider the quantity

$$I[\tilde{\rho}] := \int \tilde{\rho}(z)\ln(\tilde{\rho}(z))dz, \tag{4}$$

where $\tilde{\rho}(z)$ is the MNP density, ρ_{MNP}, with normalization $\int_0^{L_c}\tilde{\rho}(z)dz = 1$.

The obtained I as a function of the magnetic field is shown in Fig. 7. For comparison, we have also indicated the values of I for two extreme cases: $I_{\max}$, which corresponds to an absolutely uniform distribution of MNP, and $I_{\min}$, which refers to the case where all MNP are concentrated close to the walls in a region of width $\sigma_l = 3$, the length corresponding to the large axis of the particles.

For small values of H, I remains essentially equal to its value at $H = 0$, which is close to $I_{\max}$ (reflecting a nearly homogeneous distribution). Only when H becomes larger than the threshold value $\mu H \simeq 15$, I starts to decrease, indicating the onset of demixing. Moreover, the overlay of the H dependence of I and σ_{xy} in Fig. 7 shows that for larger field strengths, the stress decreases along with the I decrease. These results confirm the correlation between onset of inhomogeneity and reduction of stress.

Having established the correlation between the demixing and the decrease of the shear stress, there remains the question for the underlying physical mechanism. Our interpretation is as follows: the "misalignment" of the MNP at small fields leads to restrictions of the flow-induced motion of the nonmagnetic ones, and hence, to an increase of the stress. However, this is true only if the MNP are dispersed between the LC. As soon as the system demixes (see Figs. 6 and 7), that is, at large values of μH, the MNP are concentrated close to the walls. This provides a channel for the LC, in which they can flow without (orientational and positional) disturbances from the MNP.

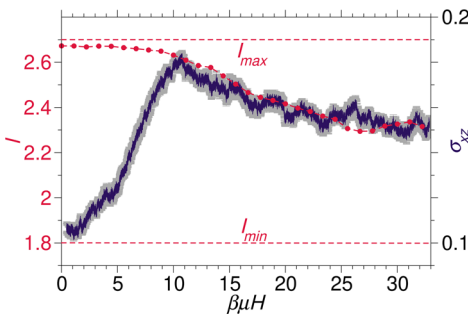

FIG. 7. The entropylike quantity of Eq. (4) as a measure of homogeneous distribution of the MNP for different values of the external magnetic field strength. The data clearly show that there is a transition from homogeneous spatial distribution of the MNP to an inhomogeneous one.

Clearly, a key ingredient in this line of argumentation is the field-induced orientational mismatch between the MNP and LC. Our numerical results indicate that this mismatch alone leads to a demixing-like transition: We emphasize that the interactions between all the particles are identical, so the demixing cannot be attributed to different shapes or interactions between the two species, such as the demixing transitions reported in Refs. 27 and 82–91. In fact, a segregation of MNP has been predicted earlier,[1] on the basis of free-energy arguments, which relies on having a distribution of nematic directors of the LC and migration of the MNP to regions where the magnetic dipoles are aligned with both, the nematic director and the external field. Our system is different from the aforementioned one, as the MNP are not "locked" to the LC nematic director (as in Ref. 1) and their orientations can actually deviate strongly [as shown in Fig. 5(b)]. We further note that the demixing also occurs in bulk simulations (where the shear is induced via the Lees-Edward boundary condition[92]), which emphasizes that the demixing is not due to the existence of the walls.

We propose that the observed demixing between particles of different orientations can be understood as a competition between mixing entropy and packing entropy. Qualitatively speaking, on the one hand, it is preferable for the system if particles with the same orientations stay close to each other as this leads to larger (orientational) free volumes for each particle. On the other hand, more (positional) configurations are available to the system if the particles are uniformly distributed in the system irrespective of their orientations. In other words, an increase in packing entropy is obtained when particles of similar orientations are neighbors, whereas higher mixing entropy is reached when particles are uniformly distributed over the whole system. In our system, at small fields, where the misalignment is not yet pronounced, the mixing entropy dominates and the MNP are uniformly distributed between the LC. In contrast, at large fields, where the misalignments are large, the system gains entropy by bringing particles of similar orientation close to each other (and hence demixing).

In Appendix D, by using a simplified Onsager analysis[93] for binary mixtures,[94] we argue that particle misalignments are, indeed, sufficient to cause demixing. We show that the free energy difference between the demixed state and the fully mixed state of long, hard ellipsoids can be written as

$$\Delta\mathscr{F} = (1-x)\ln(1-x) + x\ln(x) + 2cb_\perp x(1-x)|\sin(\Theta)|, \tag{5}$$

where c is the number density, $b_\perp$ is the excluded volume of two ellipsoids in perpendicular configuration,[93] and Θ is the angle measuring the degree of misalignment. In the present case, Θ is essentially determined by the magnetic field. We find from Eq. (5) that, there is a critical density below which mixing is favored, whereas above it, depending on the misalignment between the directions (Θ) and composition (x), demixing is favored. Although the aforementioned Onsager analysis relies on equilibrium arguments, it

does suggest that demixing in the present nonequilibrium system is possible.

Experimentally, a similar demixing has been realized in a system of nanorods,[95] where a certain degree of polydispersity is required to induce particle misalignments. In contrast to that, in our study, the demixing occurs between monodisperse particles. This isolates the role of orientational misalignments. Moreover, we want to emphasize that, in contrast to Ref. 95, being out-of-equilibrium is essential for the observed demixing in our system as one of the favored orientations is the shear-induced orientation.

IV. CONCLUSION AND OUTLOOK

In this study, we performed a NEMD study of a mixture of anisotropic magnetic and nonmagnetic particles confined between two rough solid walls, focusing on the shear stress in the presence of a continuously increasing external magnetic field. In our model, the interactions between both types of particles are the same. The only difference between the magnetic and nonmagnetic particles is that the field acts solely on the direction of the magnetic particles. Our simulation results indicate that, for a fixed shear rate and a fixed rate of increasing the magnetic field, the obtained shear stress depends on the strength and direction of the external field. More specifically, for a field direction within shear-plane and perpendicular to the shear-induced nematic director, we observe a nonmonotonic dependence of shear stress, and thus, the viscosity, on the applied field strength. By analyzing the nematic director of the LC and MNP, we have found that the increase in the shear stress is correlated with the misalignment of the MNP director relative to the shear-induced director of the majority of particles, i.e., the LC particles. The shear stress increases up to the point that the misalignment is sufficient to cause an entropic demixing between the MNP and LC. The occurrence of demixing is also (qualitatively) predicted by a simplified Onsager analysis. Unlike previously analyzed systems where the effective entropic interaction is due to size-polydispersity[27,82–84] or shape-polydispersity,[85–91] in our system the underlying mechanism is due to (competing) orientations. This is an interesting case of an effective interaction where there is no difference in shape and interparticle interaction between the particles constituting different species. This extends the notion of the directional entropic forces, introduced in Refs. 96 and 97, to a system where the particles are much simpler in their shapes.

Given the complex response observed in the present study, one would expect even more diverse behavior when dipole–dipole interaction between the MNP are included. The rheology of the MNP/LC mixture in the external magnetic field over a range of dipole–dipole couplings will be the subject of further studies. Indeed, as it is known for systems of pure anisotropic MNP, the dipole–dipole interaction can lead to self-assembled structures, which can be significantly different from the chain formation observed[31] in systems of spherical MNP. In particular, for MNP with large enough aspect ratios, the neighboring particles prefer formations with antiparallel configurations.[30,98] We speculate that such formation of a structured phase within the liquid phase has important consequences for the rheological properties of the mixture, similar to the effect of including crystalline microstructures in amorphous bulk metallic glasses.[99–101] We also expect that the external field has an important effect on the rheology. As the external field disfavors the antiparallel dipoles, the stability of the assembled structures of MNP is reduced,[30] which can lead to dissolving these structures in the liquid phase.

In this study, we only focused on the case where the dipoles are aligned with the longest axis of the ellipsoid. The anisotropic shape of the MNP also offers the possibility of aligning the magnetic dipole along different axes of the particles. For further studies, one can consider embedding the magnetic dipoles along the shortest axis, as done in recent experiments,[13] or include an offset from the center as done for spherical particles.[102–107] Depending on different embeddings, by increasing the dipole–dipole interaction strength, we speculate to find intriguing structures where an external magnetic field can play an important role in stabilizing or destabilizing them.

SUPPLEMENTARY MATERIAL

See the supplementary material for C++ files to integrate the equation of motion of the magnetic ellipsoidal particles. In these routines, it is assumed that the magnetic dipoles are embedded along their longest axis.

ACKNOWLEDGMENTS

We gratefully acknowledge funding support from the Deutsche Forschungsgemainschaft (DFG) via the priority Program No. SPP 1681.

APPENDIX A: EFFECTS OF WALLS

Strong confinement can lead to structural and dynamical properties, which are significantly different from bulk properties.[108,109] Nevertheless, if the confinement is not severe, one would expect the sample to behave similarly to the bulk. In this appendix, we argue that although the system studied here has walls and is therefore confined, the wall effects are negligible at the current wall-to-wall separation.

Prior to studying the effect of walls, it is useful to compare our bulk results with the literature results; here, we use Refs. 44 and 45. The comparison shows quantitative agreement between the nematic order parameter as a function of density (see the inset of Fig. 8). The data presented in Refs. 44 and 45 are calculated for a system with $N = 256$, and therefore, we also use a smaller system compared to the system described in Sec. II (only for the data presented in this inset). The temperature range for the coexistence of the isotropic and nematic phases at our main working density ($\rho^\star = 0.34$) is indicated by a shaded area in Fig. 8. This temperature range, which is estimated in Refs. 44 and 45, coincides with the temperature range above which the nematic ordering occurs partially in our simulations (i.e., S is larger than zero, and yet not as large as one).

To investigate the effect of confinement, we first compare the nematic order (in the absence of the magnetic field and shear) as a function of temperature for two systems: the system without walls (i.e., the system with the periodic boundary conditions in all directions), and the same system after creating walls by freezing the wall particles, as explained in the main text (see Sec. II). In Fig. 8, the nematic order of the system in the presence of wall is shown over a range of temperatures. Also indicated is the value of S at the main

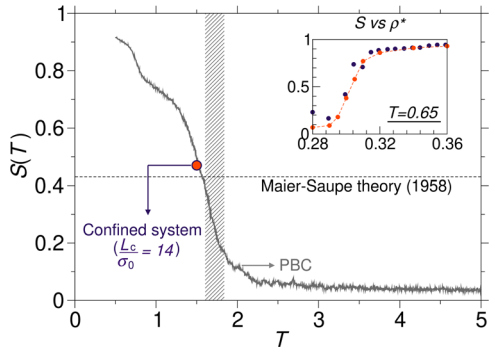

FIG. 8. Nematic order parameter as a function of temperature. The gray line pertains to the system with the full periodic boundary conditions, and the orange dot presents the value of S for the same system at $T = 1.5$, after creation of the walls, as explained in Sec. II. The horizontal dashed line represent the approximate critical nematic order parameter,[61–63] $S_c \simeq 0.43$, above which the system is considered to be in the nematic phase. The temperature range of coexistence of isotropic and nematic states[44,45] is also depicted by the dashed area. The main working temperature is chosen such that the system is very close to isotopic to nematic state transition ($S \simeq 0.45$). The inset compares the dependence of S on ρ^* with the data reprinted from Ref. 44. The inset shows that our simulation results (presented by points connected via a dashed-line) match quantitatively with the data from Ref. 44 (which is depicted by points).

working temperature, i.e., $T = 1.5$, in the presence of walls. It is seen that the change in S, as a result of introducing walls, is negligible. One should note that, as the system at $T = 1.5$ is very close to its isotropic-to-nematic transition, one would expect a relatively high sensitivity of S on the ambient changes, including introducing walls. Even under these conditions, introducing walls does not change S, which is an indication that the walls do not dominate the behavior of the system.

As a second point, we check the effect of the walls in the presence of shear flow by measuring the density and shear rate profiles across the channel (along z-direction) at different strengths of the external field. The local density is obtained as described in Sec. II, and the local shear rate is obtained by $\dot{\gamma}(z) := \frac{d}{dz}v_x(z)$, where $v_x(z_0)$ is the average x-component of velocities of all particles between planes $z = z_0 - \delta z/2$ and $z = z_0 + \delta z/2$, and $\delta z = 0.25$ is the descritization resolution along the z-axis. The obtained velocity, shear rate, and density profiles are shown in Fig. 9, for $T = 1.5$ and $\dot{\Gamma} = 5 \times 10^{-2}$. The velocity profile shows that the flow is almost independent of the magnetic field strength. This is remarkable, given that the composition profile and also the average orientations strongly depend on the magnetic field strength. The shear rate profile, plotted in the inset of Fig. 9, shows that there is no slip close to the walls, and that the wall effects on the dynamics (here, the local shear rate) reach from the wall into the bulk of the system over a length of about $\simeq 3\sigma_0$. The same is valid for the local density of all particles.

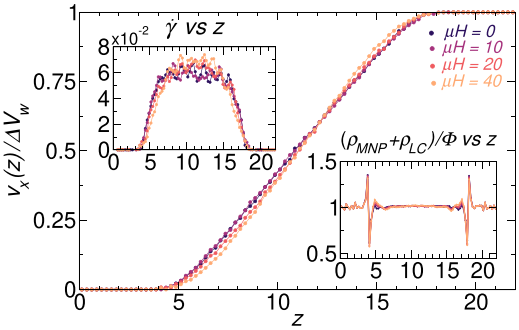

FIG. 9. The velocity profile, $v_x(z)$, which is the average velocity along x-direction as a function of z at $T = 1.5$ and four different values of μH. The local shear-rate, $\dot{\gamma}(z) = \frac{d}{dz}v_x(z)$, and the local particle density (including both MNP and LC particles) are shown in the insets. In all the above figures, $z < 4$ and $z > 4$ correspond to the wall regions. There is no indication of slip as there is no discontinuity of the shear rate across the boundary. The condition at the boundary can be approximated with no slip boundary condition, where the boundary effects are present up to $3\sigma_0$.

APPENDIX B: DEPENDENCE OF THE SHEAR STRESS ON THE FIELD PROTOCOL

In this study, as mentioned in Sec. II, the magnetic field is increased gradually from zero to $H_{\max}$ over the time interval $t_{\max}$, i.e., with the rate of $dH/dt = H_{\max}/t_{\max}$. Here, we check whether the nonmonotonic behavior, which is the subject of this study, is affected by changing the values of dH/dt. The magnetic field dependence of the shear stress is shown in Fig. 10, for a range of dH/dt values. The rates are chosen to be both larger and smaller than the rate used primarily in this work, which corresponds to $\mu dH/dt = 0.033$. Similar to the temperature dependence of shear stress (see Fig. 3), the results in Fig. 10 show that the nonmonotonic behavior is not affected at a qualitative level for the examined values of dH/dt. Nevertheless, the σ_{xz}–H curve changes quantitatively for different values of dH/dt: by increasing the aforementioned rate, the peak becomes more pronounced and the H value corresponding to the peak also increases.

Given this sensitivity, it is interesting to analyze the relevant timescales. For this purpose, we consider the two phenomena,

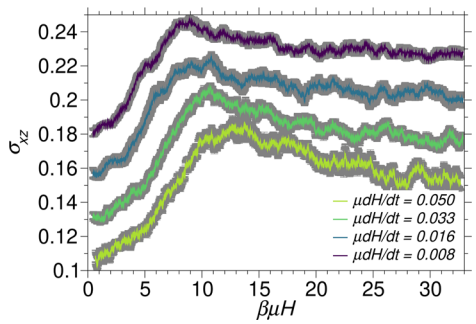

FIG. 10. Shear stress as a function of the magnetic field strength for different values of $\beta\mu dH/dt$ at $T = 1.5$ (the rate used in the main text is $\beta\mu dH/dt = 4.4 \times 10^{-3}$). For visualization purposes, the results of each $\beta\mu dH/dt$ are shifted along y-axis by 0.025 with respect to the results of the higher $\beta\mu dH/dt$ value. The results show that despite quantitative differences, the qualitative dependence of the shear stress on H does not depend on the dH/dt value (within the considered range of values).

which play important roles in the observed nonmonotonic behavior of the shear stress (see Sec. III), namely, (i) the reorientation of the MNP away from the direction of $\hat{\mathbf{n}}_0$, which leads to the increase of the shear-stress, and (ii) the translational diffusion of the MNP, which is crucial for the demixing and hence the decrease of the shear stress. We denote these timescales by τ_θ and τ_D, respectively.

For a given system, the rate $\mu dH/dt$ is considered to be large if $\tau_\theta \ll \tau_D$, i.e., the magnetic field reorients the particles faster than they can diffuse (and obtain their steady state spatial distribution), while being reoriented. On the contrary, $\mu dH/dt$ is considered to be small if τ_θ is orders of magnitude larger than τ_D, such that the particles can diffuse over the width of the channel (a process necessary for demixing). In the following, we estimate these timescales for $\mu dH/dt = 6.6 \times 10^{-3}$ (in simulation units of energy per time) to find out which of the above-mentioned scenarios occurs for this rate. We note that both τ_θ and τ_D are also affected by the shear rate. Here, we measure them for the shear rate used throughout this study, i.e., $\dot{\Gamma} = 5 \times 10^{-2}$.

We estimate τ_θ via measuring the time required for $\hat{\mathbf{n}}_{\mathrm{MNP}}$ to change its orientation from $\hat{\mathbf{n}}_0$ to $\hat{\mathbf{H}}$. For the rate which is primarily used in the main text (i.e., $\mu dH/dt = 6.6 \times 10^{-3}$), one can obtain τ_θ from Fig. 5(b). The data suggest that $\hat{\mathbf{n}}_{\mathrm{MNP}}$ changes significantly as $\beta\mu H$ changes from 3 to 13, which corresponds to a time interval of $\tau_\theta \simeq 2 \times 10^3$ (in simulation time units).

To estimate the translational diffusion timescale, τ_D, we measure the mean square displacement (MSD) along the z-direction (i.e., the direction of confinement) as a function of time. We measured this quantity for both species, i.e., $\alpha \in \{\mathrm{MNP}, \mathrm{LC}\}$, via $\mathrm{MSD}_{\alpha,z}(t) := 1/N_\alpha \sum_{i=1}^{N_\alpha} (z_{\alpha,i}(t) - z_{\alpha,i}(0))^2$, where $z_{\alpha,i}(t)$ is the z-component of the position of the ith particle of type α at time t. The z-component of MSD is particularly interesting for our purpose as the demixing occurs along this direction (see the lower panel of Figs. 3 and 6). One should note that the MSD calculations are performed at $H = 0$ in the steady state under shear. We estimated τ_D as the time that particles move (on average) with their own size along the z-direction, i.e., $\mathrm{MSD}_{\alpha,z}(t) = 1$. As indicated by the dashed lines in Fig. 11, the time associated with this displacement is $\tau_D \simeq 100$.

The obtained τ_D is neither much smaller nor significantly larger than τ_θ, i.e., the particles can diffuse over τ_θ but they cover a distance of $\simeq 3\sigma$, which is smaller than the channel width. This similarity of timescales suggest that for the chosen value of $\mu dH/dt$, both of the aforementioned phenomena are relevant in our system and the behavior of the system emerges as an interplay between them.

To find out if the nonmonotonic behavior survives in the limit $dH/dt \to 0$, i.e., in the steady state, a more systematic study is required. Due to the complexity of the system, the investigation of the steady-state behavior for a wide range of field strength would, indeed, imply very large computational time. Nevertheless, we speculate that the nonmonotonic behavior persists in the steady state. Based on the equilibrium Onsager analysis presented in Appendix D, the demixing occurs beyond a certain misalignment; up to the field strength corresponding to that misalignment, the stress increases. By further increase of the field strength, the stress decreases which is due to the demixing. Hence, a nonmonotonic behavior is anticipated.

APPENDIX C: STRESS AUTOCORRELATION FUNCTION

Applying shear as an external perturbation leads to the response of the system in the form of an increase of the shear stress. In the liquid phase, there is a finite characteristic time, usually referred to as the relaxation time, which the system needs to adapt to the induced stress (i.e., to reduce it to zero). This relaxation time is used to distinguish between high and low shear rates: if the inverse shear rate is much larger than the relaxation time, the applied shear rate is considered to be slow compared to the relaxation of the system and one would expect a linear response of the system. Here, we calculate the relaxation time associated with stress, τ_σ. In order to calculate such a relaxation time, we analyze the stress autocorrelation, $C_\sigma(t) := \langle \sigma_{xz}(t)\sigma_{xz}(0)\rangle / \langle \sigma_{xz}^2(0)\rangle$, which is calculated in the absence of shear. Here, $\langle\cdot\rangle$ refers to an ensemble average. As shown in Fig. 12, the stress autocorrelation decays to zero and one can assign an approximate time to this decay. For $T = 1.5$, the obtained relaxation time is $\tau_\sigma \simeq 1$.

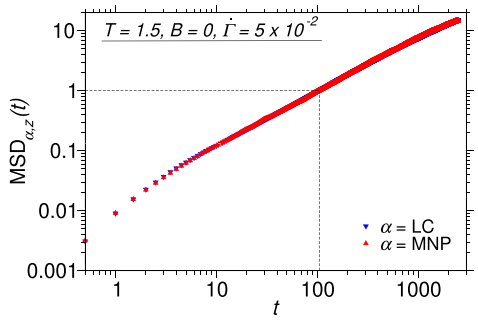

FIG. 11. The mean square displacement along the z-direction for particles of type $\alpha \in \{\mathrm{MNP}, \mathrm{LC}\}$ as a function of time. The horizontal dashed line (and its corresponding vertical line) indicates where the particle moves over the distance of σ_s (and the corresponding time, τ_D). The displacements are calculated in the presence of shear and in the absence of the magnetic field.

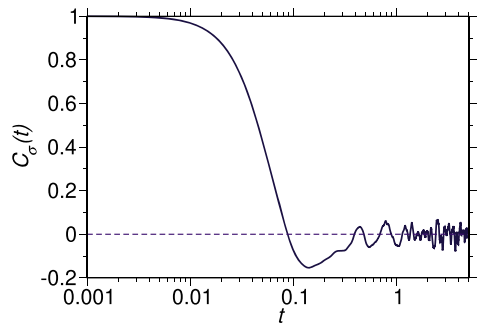

FIG. 12. The shear stress autocorrelation function, measured at $T = 1.5$ and in the absence of shear, which shows that after time $t \simeq 1$, the stress autocorrelation decays to zero.

APPENDIX D: SIMPLIFIED ONSAGER ANALYSIS

In this appendix, by using a simplified version of the Onsager analysis presented in Refs. 93 and 94, we show that for a system composed of hard ellipsoids of identical shapes, an orientational misalignment between the particles is sufficient to cause a demixing. More specifically, we consider a system composed of two particle species A and B, and the corresponding one-particle orientation distribution functions, f_A and f_B. We show that under certain constrains, the free-energy of the system is minimized if the two particle species are spatially demixed.

For simplicity and without loss of generality, we assume that f_A and f_B are given by the Dirac delta distribution located at $\hat{\mathbf{n}}_A$ and $\hat{\mathbf{n}}_B$, i.e., the average nematic directions. We also assume a canonical ensemble with total fixed particle number $N = N_A + N_B$, volume V, and temperature T, where N_A and N_B are the numbers of particles in species A and B. We are interested in the free energy of the system when (i) both particle species are homogeneously distributed ($F_{\text{hom.}}$), and (ii) particles of different species are separated from each other completely ($F_{\text{inh.}}$).

Following Ref. 94, the reduced free energy per particle for a spatially homogeneous distribution, i.e., $\mathscr{F}_{\text{hom.}} = F_{\text{hom.}}/(Nk_BT)$, reads

$$\begin{aligned}\mathscr{F}_{\text{hom.}} &= 1 + \ln(c) + (1-x)\ln(1-x) + x\ln(x) + (1-x)\sigma[f_A] \\ &\quad + x\sigma[f_B] + cb_{\parallel}(1-x)^2\rho[f_A,f_A] + cb_{\parallel}x^2\rho[f_B,f_B] \\ &\quad + 2cb_{\perp}x(1-x)\rho[f_A,f_B],\end{aligned} \tag{D1}$$

where x is the fraction of B particles, $c = N/V$ is the overall number density, $b_{\parallel} = \pi/L^2D$, and $b_{\perp} \simeq L^2D$, with $b_{\parallel}$ and $b_{\perp}$ being the excluded volumes of two long ellipsoids of length L and diameter D in parallel and perpendicular configurations.[93] In the above equation, the functional $\sigma[f]$ measures the entropy associated with the distribution f itself, and $\rho[f,f']$ measures the entropy associated with the volume available to neighboring particles with two distributions f and f' (the exact expressions can be found in Onsager's work[93]). Assuming $L \gg D$, that is, a needlelike shape, $\mathscr{F}_{\text{hom.}}$ can be approximated by

$$\begin{aligned}\mathscr{F}_{\text{hom.}} &= 1 + \ln(c) + (1-x)\ln(1-x) + x\ln(x) \\ &\quad + 2cb_{\perp}x(1-x)|\sin(\Theta)|,\end{aligned} \tag{D2}$$

where Θ is the angle between $\hat{\mathbf{n}}_A$ and $\hat{\mathbf{n}}_B$. Similarly, we obtain a reduced free energy for the case where the species A and B are spatially separated. In this case, the free energy per particle for each of the species is obtained by setting x to zero, as each phase is purely composed of one species. This leads to

$$\mathscr{F}_{\text{inh.}} = 1 + \ln(c), \tag{D3}$$

where the free-energy associated with the boundary between the two species is neglected. The difference between the free energies in the demixed state and that in the mixed state, $\Delta\mathscr{F} = \mathscr{F}_{\text{inh.}} - \mathscr{F}_{\text{hom.}}$, is given by

$$\Delta\mathscr{F} = (1-x)\ln(1-x) + x\ln(x) + 2cb_{\perp}x(1-x)|\sin(\Theta)|. \tag{D4}$$

The first two terms on the right side of Eq. (D4) are always negative, and thus, favor a mixed system, while the third term is always positive, and thus, favors demixing. The magnitude of the third term increases by increasing Θ, which might eventually lead to a sign change for $\Delta\mathscr{F}$. It is straightforward to show that, depending on the values of Θ and x, $\Delta\mathscr{F}$ can become positive. In particular, one can show that there is a critical density c_{cr} [with $c_{\text{cr}}b_{\perp} = 2\ln(2)$], below which mixing is always favored.

REFERENCES

[1] F. Brochard and P. de Gennes, J. Phys. **31**, 691 (1970).
[2] J. Rault, P. Cladis, and J. Burger, Phys. Lett. A **32**, 199 (1970).
[3] A. Mertelj, D. Lisjak, M. Drofenik, and M. Čopič, Nature **504**, 237 (2013).
[4] A. Mertelj, N. Osterman, D. Lisjak, and M. Čopič, Soft Matter **10**, 9065 (2014).
[5] Q. Liu, P. J. Ackerman, T. C. Lubensky, and I. I. Smalyukh, Proc. Natl. Acad. Sci. U. S. A. **113**, 10479 (2016).
[6] N. Podoliak, O. Buchnev, D. V. Bavykin, A. N. Kulak, M. Kaczmarek, and T. J. Sluckin, J. Colloid Interface Sci. **386**, 158 (2012).
[7] P. Kopčanský, N. Tomašovičová, M. Koneracká, V. Závišová, M. Timko, A. Džarová, A. Šprincová, N. Éber, K. Fodor-Csorba, T. Tóth-Katona *et al.*, Phys. Rev. E **78**, 011702 (2008).
[8] S. D. Peroukidis, K. Lichtner, and S. H. Klapp, Soft Matter **11**, 5999 (2015).
[9] S. D. Peroukidis and S. H. Klapp, Phys. Rev. E **92**, 010501(R) (2015).
[10] S.-H. Chen and N. M. Amer, Phys. Rev. Lett. **51**, 2298 (1983).
[11] A. V. Kyrylyuk, M. C. Hermant, T. Schilling, B. Klumperman, C. E. Koning, and P. Van der Schoot, Nat. Nanotechnol. **6**, 364 (2011).
[12] O. Buluy, S. Nepijko, V. Reshetnyak, E. Ouskova, V. Zadorozhnii, A. Leonhardt, M. Ritschel, G. Schönhense, and Y. Reznikov, Soft Matter **7**, 644 (2011).
[13] F. Martinez-Pedrero, A. Cebers, and P. Tierno, Phys. Rev. Appl. **6**, 034002 (2016).
[14] S. Kredentser, M. Kulyk, V. Kalita, K. Slyusarenko, V. Y. Reshetnyak, and Y. A. Reznikov, Soft Matter **13**, 4080 (2017).
[15] N. Sebastián, N. Osterman, D. Lisjak, M. Čopič, and A. Mertelj, Soft Matter **14**, 7180 (2018).
[16] T. Potisk, A. Mertelj, N. Sebastián, N. Osterman, D. Lisjak, H. R. Brand, H. Pleiner, and D. Svenšek, Phys. Rev. E **97**, 012701 (2018).
[17] G. Zarubin, M. Bier, and S. Dietrich, Soft Matter **14**, 9806 (2018).
[18] G. Zarubin, M. Bier, and S. Dietrich, J. Chem. Phys. **149**, 054505 (2018).
[19] R. Blaak, S. Auer, D. Frenkel, and H. Löwen, J. Phys.: Condens. Matter **16**, S3873 (2004).
[20] M. Ripoll, P. Holmqvist, R. Winkler, G. Gompper, J. Dhont, and M. Lettinga, Phys. Rev. Lett. **101**, 168302 (2008).
[21] A. V. Mokshin and J.-L. Barrat, Phys. Rev. E **77**, 021505 (2008).
[22] S. Mandal, M. Gross, D. Raabe, and F. Varnik, Phys. Rev. Lett. **108**, 098301 (2012).
[23] G. P. Shrivastav, P. Chaudhuri, and J. Horbach, J. Rheol. **60**, 835 (2016).
[24] N. Kikuchi and J. Horbach, Europhys. Lett. **77**, 26001 (2007).
[25] E. Zaccarelli, S. M. Liddle, and W. C. Poon, Soft Matter **11**, 324 (2015).
[26] D. Heckendorf, K. Mutch, S. Egelhaaf, and M. Laurati, Phys. Rev. Lett. **119**, 048003 (2017).
[27] C. Ferreiro-Córdova and H. Wensink, J. Chem. Phys. **145**, 244904 (2016).
[28] A. Verhoeff, H. Wensink, M. Vis, G. Jackson, and H. Lekkerkerker, J. Phys. Chem. B **113**, 13476 (2009).
[29] A. Speranza and P. Sollich, J. Chem. Phys. **117**, 5421 (2002).
[30] C. E. Alvarez and S. H. Klapp, Soft Matter **8**, 7480 (2012).
[31] H. Schmidle, C. K. Hall, O. D. Velev, and S. H. Klapp, Soft Matter **8**, 1521 (2012).
[32] A. Sreekumari and P. Ilg, Phys. Rev. E **88**, 042315 (2013).
[33] K. May, A. Eremin, R. Stannarius, S. D. Peroukidis, S. H. Klapp, and S. Klein, Langmuir **32**, 5085 (2016).
[34] S. D. Peroukidis and S. H. Klapp, Soft Matter **12**, 6841 (2016).
[35] G. P. Shrivastav and S. H. Klapp, Soft Matter **15**, 973 (2019).
[36] S. Odenbach, J. Phys.: Condens. Matter **16**, R1135 (2004).

[37]R. Rosensweig, R. Kaiser, and G. Miskolczy, J. Colloid Interface Sci. **29**, 680 (1969).
[38]W. Hall and S. Busenberg, J. Chem. Phys. **51**, 137 (1969).
[39]M. Shliomis, Zh. Eksp. Teor. Fiz. **61**, 2411–2418 (1972).
[40]R. Berardi, C. Fava, and C. Zannoni, Chem. Phys. Lett. **297**, 8 (1998).
[41]S. Plimpton, J. Comput. Phys. **117**, 1 (1995).
[42]L. Verlet, Phys. Rev. **159**, 98 (1967).
[43]W. C. Swope, H. C. Andersen, P. H. Berens, and K. R. Wilson, J. Chem. Phys. **76**, 637 (1982).
[44]E. De Miguel, L. F. Rull, M. K. Chalam, and K. E. Gubbins, Mol. Phys. **74**, 405 (1991).
[45]J. T. Brown, M. P. Allen, E. M. del Río, and E. de Miguel, Phys. Rev. E **57**, 6685 (1998).
[46]N. H. Siboni, D. Raabe, and F. Varnik, Phys. Rev. E **87**, 030101 (2013).
[47]F. Varnik, L. Bocquet, J.-L. Barrat, and L. Berthier, Phys. Rev. Lett. **90**, 095702 (2003).
[48]M. Hassani, P. Engels, and F. Varnik, Europhys. Lett. **121**, 18005 (2018).
[49]D. J. Evans and G. P. Morriss, Phys. Rev. Lett. **56**, 2172 (1986).
[50]P. A. Thompson and M. O. Robbins, Phys. Rev. Lett. **63**, 766 (1989).
[51]P. A. Thompson and M. O. Robbins, Phys. Rev. A **41**, 6830 (1990).
[52]T. Soddemann, B. Dünweg, and K. Kremer, Phys. Rev. E **68**, 046702 (2003).
[53]X. Zhou, D. Andrienko, L. Delle Site, and K. Kremer, Europhys. Lett. **70**, 264 (2005).
[54]F. Varnik, J. Chem. Phys. **125**, 164514 (2006).
[55]A. Niavarani and N. V. Priezjev, Phys. Rev. E **77**, 041606 (2008).
[56]D. S. Bolintineanu, J. B. Lechman, S. J. Plimpton, and G. S. Grest, Phys. Rev. E **86**, 066703 (2012).
[57]K. S. Cheung and S. Yip, J. Appl. Phys. **70**, 5688 (1991).
[58]B. Todd, D. J. Evans, and P. J. Daivis, Phys. Rev. E **52**, 1627 (1995).
[59]F. Schwabl and W. D. Brewer, *Statistical Mechanics*, 2nd ed. (Springer Science & Business Media, Berlin, Heidelberg, 2006).
[60]F. M. Leslie, Arch. Ration. Mech. Anal. **28**, 265 (1968).
[61]W. Maier and A. Saupe, Z. Naturforsch. A **13**, 564 (1958).
[62]W. Maier and A. Saupe, Z. Naturforsch. A **14**, 882 (1959).
[63]W. Maier and A. Saupe, Z. Naturforsch. A **15**, 287 (1960).
[64]M. Miesowicz, Nature **158**, 27 (1946).
[65]S. Hess and M. Kröger, J. Phys.: Condens. Matter **16**, S3835 (2004).
[66]C. Wu, T. Qian, and P. Zhang, Liq. Cryst. **34**, 1175 (2007).
[67]V. Fréedericksz and A. Repiewa, Z. Phys. **42**, 532 (1927).
[68]V. Fréedericksz and V. Zolina, Trans. Faraday Soc. **29**, 919 (1933).
[69]G. B. Jeffery, Proc. R. Soc. London, Ser. A **102**, 161 (1922).
[70]F. H. Stillinger, Science **267**, 1935 (1995).
[71]F. H. Stillinger and T. A. Weber, Phys. Rev. A **25**, 978 (1982).
[72]B. Doliwa and A. Heuer, Phys. Rev. E **67**, 030501 (2003).
[73]M. L. Falk and J. S. Langer, Phys. Rev. E **57**, 7192 (1998).
[74]I. Goldhirsch and C. Goldenberg, Eur. Phys. J. E **9**, 245 (2002).
[75]E. Rabani, J. D. Gezelter, and B. J. Berne, J. Chem. Phys. **107**, 6867 (1997).
[76]F. A. Lindemann, Phys. Z. **11**, 609 (1910).
[77]J. W. Ahn, B. Falahee, C. Del Piccolo, M. Vogel, and D. Bingemann, J. Chem. Phys. **138**, 12A527 (2013).
[78]N. H. Siboni, D. Raabe, and F. Varnik, Europhys. Lett. **111**, 48004 (2015).
[79]G. Adam and J. H. Gibbs, J. Chem. Phys. **43**, 139 (1965).
[80]R. Richert and C. Angell, J. Chem. Phys. **108**, 9016 (1998).
[81]J. C. Mauro, Y. Yue, A. J. Ellison, P. K. Gupta, and D. C. Allan, Proc. Natl. Acad. Sci. U. S. A. **106**, 19780 (2009).
[82]K. R. Purdy, S. Varga, A. Galindo, G. Jackson, and S. Fraden, Phys. Rev. Lett. **94**, 057801 (2005).
[83]S. Varga, K. Purdy, A. Galindo, S. Fraden, and G. Jackson, Phys. Rev. E **72**, 051704 (2005).
[84]M. A. Bates and D. Frenkel, J. Chem. Phys. **110**, 6553 (1999).
[85]L. Helden, R. Roth, G. H. Koenderink, P. Leiderer, and C. Bechinger, Phys. Rev. Lett. **90**, 048301 (2003).
[86]R. Roth, J. Brader, and M. Schmidt, Europhys. Lett. **63**, 549 (2003).
[87]J. M. Brader, A. Esztermann, and M. Schmidt, Phys. Rev. E **66**, 031401 (2002).
[88]M. Tasinkevych and D. Andrienko, Eur. Phys. J. E **21**, 277 (2006).
[89]J. K. Whitmer, A. A. Joshi, T. F. Roberts, and J. J. de Pablo, J. Chem. Phys. **138**, 194903 (2013).
[90]M. Adams, Z. Dogic, S. L. Keller, and S. Fraden, Nature **393**, 349 (1998).
[91]N. Mizoshita, K. Hanabusa, and T. Kato, Adv. Funct. Mater. **13**, 313 (2003).
[92]A. Lees and S. Edwards, J. Phys. C: Solid State Phys. **5**, 1921 (1972).
[93]L. Onsager, Ann. N. Y. Acad. Sci. **51**, 627 (1949).
[94]H. N. W. Lekkerkerker, P. Coulon, R. Van Der Haegen, and R. Deblieck, J. Chem. Phys. **80**, 3427 (1984).
[95]E. Van den Pol, A. Lupascu, M. Diaconeasa, A. Petukhov, D. Byelov, and G. Vroege, J. Phys. Chem. Lett. **1**, 2174 (2010).
[96]P. F. Damasceno, M. Engel, and S. C. Glotzer, ACS Nano **6**, 609 (2011).
[97]G. van Anders, N. K. Ahmed, R. Smith, M. Engel, and S. C. Glotzer, ACS Nano **8**, 931 (2013).
[98]S. C. McGrother, A. Gil-Villegas, and G. Jackson, Mol. Phys. **95**, 657 (1998).
[99]D. C. Hofmann, J.-Y. Suh, A. Wiest, G. Duan, M.-L. Lind, M. D. Demetriou, and W. L. Johnson, Nature **451**, 1085 (2008).
[100]C. Hays, C. Kim, and W. L. Johnson, Phys. Rev. Lett. **84**, 2901 (2000).
[101]W. Guo, E. A. Jägle, P.-P. Choi, J. Yao, A. Kostka, J. M. Schneider, and D. Raabe, Phys. Rev. Lett. **113**, 035501 (2014).
[102]S. Kantorovich, R. Weeber, J. J. Cerda, and C. Holm, Soft Matter **7**, 5217 (2011).
[103]M. Klinkigt, R. Weeber, S. Kantorovich, and C. Holm, Soft Matter **9**, 3535 (2013).
[104]D. Morphew and D. Chakrabarti, Soft Matter **12**, 9633 (2016).
[105]G. Steinbach, S. Gemming, and A. Erbe, Eur. Phys. J. E **39**, 69 (2016).
[106]A. B. Yener and S. H. Klapp, Soft Matter **12**, 2066 (2016).
[107]D. M. Rutkowski, O. D. Velev, S. H. Klapp, and C. K. Hall, Soft Matter **13**, 3134 (2017).
[108]T. Gruhn and M. Schoen, Phys. Rev. E **55**, 2861 (1997).
[109]M. G. Mazza, M. Greschek, R. Valiullin, J. Kärger, and M. Schoen, Phys. Rev. Lett. **105**, 227802 (2010).